Accepted Manuscript

Dual triggers induced disassembly of DNA polymer decorated silver nanoparticle for ultrasensitive electrochemical Pb^{2+} detection

Xiyue Xie, Yaqin Chai, Yali Yuan, Ruo Yuan

PII: S0003-2670(18)30815-8

DOI: 10.1016/j.aca.2018.06.050

Reference: ACA 236065

To appear in: *Analytica Chimica Acta*

Received Date: 27 April 2018

Revised Date: 12 June 2018

Accepted Date: 15 June 2018

Please cite this article as: X. Xie, Y. Chai, Y. Yuan, R. Yuan, Dual triggers induced disassembly of DNA polymer decorated silver nanoparticle for ultrasensitive electrochemical Pb^{2+} detection, *Analytica Chimica Acta* (2018), doi: 10.1016/j.aca.2018.06.050.

Graphical Abstract

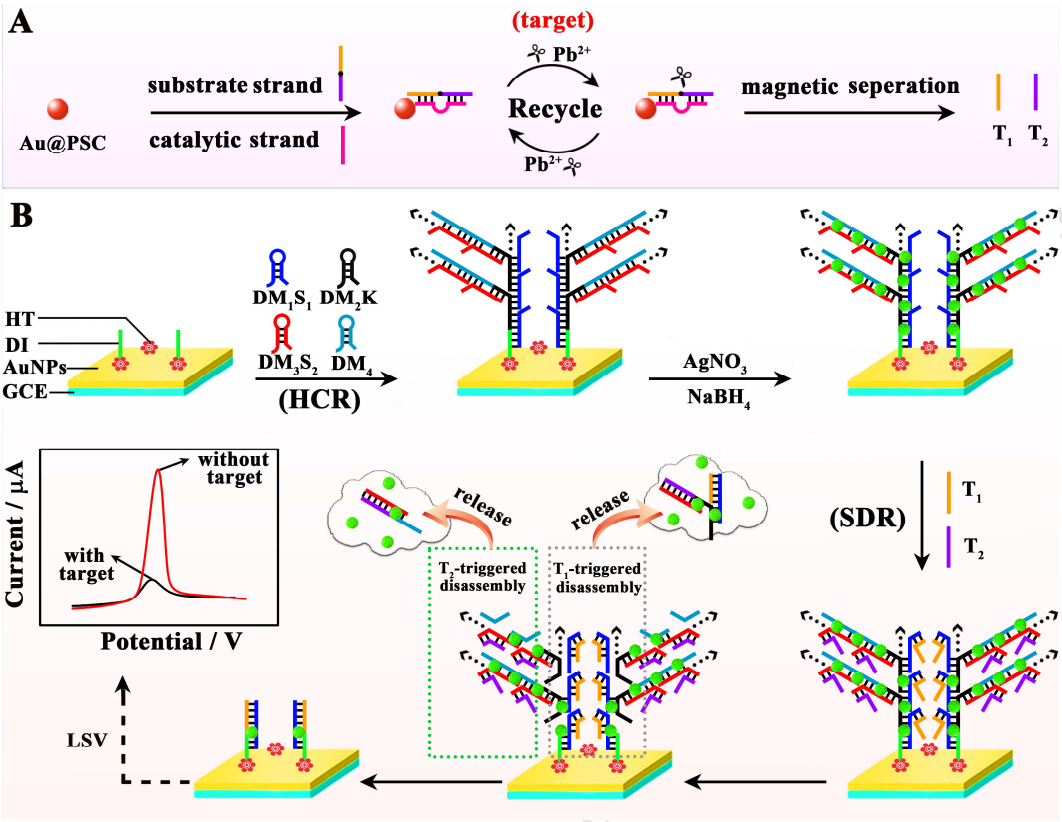

Dual triggers induced disassembly of DNA polymer decorated silver nanoparticle for ultrasensitive electrochemical Pb^{2+} detection

Xiyue Xie, Yaqin Chai, Yali Yuan, Ruo Yuan**

Key Laboratory of Luminescent and Real-Time Analytical Chemistry (Southwest University), Ministry of Education, College of Chemistry and Chemical Engineering, Southwest University, Chongqing 400715, PR China

Abstract

In this work, a new label-free biosensor based on highly effective decomposition of a branched DNA polymer and target-transition recycling amplification was designed for ultrasensitive electrochemical determination of lead ion (Pb^{2+}). The branched DNA polymer formed by hybridization chain reaction (HCR) was first immobilized on electrode and served as the carrier for loading abundant silver nanoparticle (AgNPs) to generate an extremely high initial current signal output. Then, the molecular triggers T_1 and T_2, which were produced through a target-transition recycling amplification, could respectively disassemble the backbone and side chain of the branched DNA polymer with remarkably decreased current for sensitive detection of Pb^{2+}. Compared with traditional one-trigger induced disassembly strategy, the proposed approach exhibited higher decomposition efficiency. The experimental data showed that this developed biosensor had a superior performance for Pb^{2+} detection with a low detection limit down to 0.24 pM. Furthermore, the established

* Corresponding author. Tel.: +86-23-68252277; Fax: +86-23-68253172.

E-mail address: y198688@swu.edu.cn (Y. L. Yuan); yuanruo@swu.edu.cn (R. Yuan)

strategy set up a new way to achieve the ultrasensitive detection of metal ions.

Keywords: branched DNA polymer; dual triggers induced disassembly; high decomposition efficiency; strand displacement reaction.

1. Introduction

Branched DNA polymer, as one of the typical natural polymer commonly formed in a "bottom-up" assembly mode through polymerase chain reaction (PCR) [1], rolling circle amplification (RCA) [2], hybridization chain reaction (HCR) etc. [3-5], has attracted increasing attention owing to its superior biocompatibility and programmable structure, and thus be widely applied in the field of electrochemiluminescent [6], fluorescent [7], photoelectrochemical [8], especially electrochemical biosensors [9] for the detection of various targets including small molecules, nucleic acids and proteins. Since the branched DNA polymer composed by vast DNA strands contains abundant repeat units, large number of binding sites can be provided for assembling signal probes such as methylene blue [10], ferrocene [11] and $[Ru(NH_3)_6]^{3+}$ [12] with significantly improved sensitivity. More importantly, the branched DNA polymer inherently possesses the desirable reversibility of forming and decomposition [13,14], furnishing a possibility of constructing a biosensor based on the decomposition of branched DNA polymer with extremely high initial signal.

Up to now, the decomposition of branched DNA polymer has been mainly performed by increasing temperature or using DNase. [15] Nevertheless, these methods exhibit a fatal defect of unwinding a certain DNA polymer without selectivity. By contrast, strand displacement reaction (SDR) as a physiological, selective, and enzyme-free disassembly strategy for controlling DNA polymer disassembly has been developed to resolve the above-mentioned problem. [16-18]

Therefore, it can be feasible to design a single-stranded DNA that disassembles branched DNA polymer through hybridizing its bottom DNA on electrode surface, but suffers from relatively weak depolymerization efficiency. [19-21] This may be due to the steric hindrance between tremendous DNA branched structure and supported platform, as well as the fact that the limited trigger DNA disassembles the branched DNA polymer with a slow speed. Hence, exploring an effective strategy that can disassemble DNA polymer with high disassembly efficiency is urgently desired. Compared with above-mentioned traditional one-trigger induced disassembly strategy, once multichannel dissociations can be simultaneously achieved during the depolymerization of branched polymer from outside to inside, which is able to overcome the aforementioned shortcomings and the decomposition efficiency would be tremendously enhanced. [22]

Inspired by the above-mentioned points, a new path for ultrasensitive Pb^{2+} detection was established in this work by combining DNAzyme assisted target recycling and controllably efficient disassembly of branched DNA polymer induced by SDR. As shown in Scheme 1, the branched DNA polymer was first constructed on electrode through HCR, which could offer an ideal platform for the immobilization of outstanding electrochemical signal tag silver nanoparticles (AgNPs). Meanwhile, the target Pb^{2+} circularly activate the cleavage of substrate strand in Pb^{2+}-specific DNAzyme with high specificity to generate large quantities of released substrate fragments (T_1 and T_2). [23,24] Coincidentally, the released T_1 and T_2 could respectively decompose the backbone and side chain in preformed branched DNA polymer, which largely improved the disassembling efficiency compared with traditional one-trigger induced disassembly strategy. As a result, the signal indicator AgNPs embedded in DNA double-strand was dissociated from electrode surface,

leading to an obvious decreased current and further dramatically improving the detection performance. The established assay opens up an innovative avenue for sensitive determination of various targets such as metal ions, protein and DNA.

(Scheme 1)

2. Experimental section

2.1 Materials and reagents

Chloroauric acid ($HAuCl_4$) and hexanethiol (HT) were bought from Sigma-Aldrich Co. (St. Louis, MO, USA). Trisodium citrate ($C_6H_5Na_3O_7 \cdot 2H_2O$) and sodium borohydride ($NaBH_4$) were ordered from Kelong Chemical Co. (Chengdu, China). Silver nitrate ($AgNO_3$) and lead nitrate ($Pb(NO_3)_2$) were commercially available from Sinopharm Chemical Reagent Ltd. (Shanghai, China). Amino-modified magnetic polystyrene microspheres (PSC) were provided by Baseline Chrom Tech Research Co. (Tianjin, China). All involved oligonucleotides were custom-synthesized by Sangon Inc. (Shanghai, China), and their sequences were given in Table 1. The base sequences marked with the same color were complementary with each other.

(Table 1)

2.2. Instruments

All electrochemical measurements including linear sweep voltammetry (LSV), cyclic voltammetry (CV) and electrochemical impedance spectroscopic (EIS) were

performed using a CHI 660D electrochemical workstation (Chenhua, Shanghai, China). LSV measurement was monitored in 1.0 M KCl solution with -0.2 ~ 0.2 V potential scan range. CV and EIS involved in the whole experiment process was performed in 2 mL mixture comprising 5 mM $K_3[Fe(CN)_6]/K_4[Fe(CN)_6]$.

2.3. Synthesis of DNAzyme-functionalized magnetic composites

First, gold nanoparticles (AuNPs) with 16 nm in diameter were synthesized on the basis of previous protocol. [25] Afterward, 5 mL AuNPs was subjected to 1 mL the NH_2-modified PSC magnetic solution and reacted for 2 h at 4 ^oC *via* Au-N bonding for synthesizing AuNPs@PSC magnetic composites. Furthermore, in order to obtain Pb^{2+}-dependent DNAzyme, 20 μL AuNPs@PSC magnetic composites were initially blended with 20 μL catalytic strands (2 μM), and the resulting mixture reacted for 12 h at 37 °C. After magnetic separation, 20 μL substrate strands (2 μM) were added into the above magnetic composites and hybridized with catalytic strands in magnetic bead to form a specific DNAzyme for Pb^{2+}. The DNAzyme functionalized magnetic composites were then separated by magnet.

2.4. Electrochemical detection of Pb^{2+}

Prior to use, four hairpin DNA monomers (DM_1S_1, DM_2K, DM_3S_2 and DM_4) were annealed at 95 °C for 5 min and subsequently cooled to room temperature for 1 h. [26,27] The 5 μL of 0.25 μM DNA initiator (DI) was first pipetted onto the cleaned electrode and incubated overnight at 4 °C. Subsequently, to reduce nonspecific adsorption of modified electrode, 15 μL HT (1.0 mM) was cast onto above electrode

for 40 min at room temperature. After washing with distilled water, the electrode was treated with 20 μL of the DNA monomers mixture including 2.5 μM DM_1S_1, DM_2K, DM_3S_2 and DM_4 (1:1:1:1) for 2 h at 37 °C to form the branched DNA polymer. Then, 10 μL $AgNO_3$ solution (100 μM) and 10 μL freshly prepared $NaBH_4$ solution (1 mM) was coated on electrode for 30 min at room temperature in the dark successively, which could reduce Ag^+ to generate numerous AgNPs on the DNA skeleton for electrochemical signal output. At the same time, when the formative Pb^{2+}-DNAzyme encountered target Pb^{2+}, the substrate strand of DNAzyme was cleaved into two parts, releasing dual triggers T_1 and T_2. After that, the above released triggers (T_1 and T_2) was dropped on electrode and incubated at 37 °C for 2 h, which leaded to the disassembly of preformed branched DNA polymer, accompanied by the release of the signal indicator. The electrode was finally rinsed in ultrapure water and then subjected to the LSV measurements in 1.0 M KCl solution.

3. Results and discussion

3.1. Characterization of the electrochemical sensing platform.

Here, the modification procedure of electrode was characterized by CV in 5 mM $[Fe(CN)_6]^{3-/4-}$ solution at a potential range from 0.2 to 0.6 V. As displayed in Fig. 1A, the pretreated GCE exhibited a couple of reversible redox peak (curve a). With the electro-deposition of AuNPs, the current response increased owing to the favorable conductivity of AuNPs (curve b). Due to the negative charge on the phosphate backbone of DNA influenced the movements of $[Fe(CN)_6]^{3-/4-}$, an obviously

decreased peak current (curve c) was emerged after DI was assembled onto electrode. Then the surface-blocking procedure with HT generated a decrease of current (curve d). The peak current further declined after incubation with mixture of DM_1S_1, DM_2K, DM_3S_2 and DM_4 (curve e), demonstrating the successful hybridization of the four DNA hairpin monomers and DI to form branched DNA polymer. Followed by the incubation of released triggers T_1 and T_2, an apparent increase of the peak current was detected (curve f), which was ascribed to the disassembly of branched DNA and the release of DNA fragment from electrode surface.

Furthermore, EIS measurement was employed to characterize the biosensor fabrication process in $[Fe(CN)_6]^{3-/4-}$ (5 mM) solution containing KCl (0.1 M). As displayed in Fig. 1B, the bare GCE displayed a small semicircle (curve a). When the AuNPs were deposited on the GCE, the value of impedance decreased significantly, suggesting the excellent conductivity of AuNPs (curve b). Afterwards, with the successive immobilization of DI, HT and four DNA hairpin monomers (DM_1S_1, DM_2K, DM_3S_2 and DM_4), the impedance values increased in order (curve c-e). One potential reason might be that the DI, HT and DNA hairpin monomers significantly hinder electron transfer. However, after the strand displacement reaction was triggered by dual triggers T_1 and T_2, the decrease of impedance value was caused by the dissociation of branched DNA polymer on electrode (curve f).

(Fig. 1)

3.2. Optimization of the assay conditions

To obtain better detection performance of the biosensor, some experimental parameters including cleavage time of Pb^{2+} and incubation time of triggers (T_1 and T_2) were optimized. In the process of DNAzyme-assisted target recycling, cleaving time was the crucial factor that influenced the cleaving effect. As shown in Fig 2A, with the increasing of incubation time, the response currents for 10 nM Pb^{2+} tended to a steady value at 80 min. Therefore, 80 min was selected as the optimal time for the cleavage of Pb^{2+}.

In addition, the incubation time of triggers (T_1 and T_2) was also an important parameter that influenced the signal response. The branched DNA polymer could be disassembled into DNA monomer units by triggers T_1 and T_2 and the DNA monomer thus released from electrode surface. Therefore, more T_1 and T_2 could depolymerize more branched DNA polymer, which further resulted in the release of electroactive material AgNPs for low signal response. As can be seen from Fig 2B, the current signal decreased along with the increase of the incubation time of triggers and reached a plateau after 120 min, suggesting that 120 min was the optimal time for the dissociation of branched DNA polymer.

(Fig. 2)

3.3. Comparison of different dissociation approach

In order to verify the high decomposition efficiency of proposed strategy, contrast experiments of biosensors were performed through the comparison of current response after incubating different molecule triggers on the electrodes. As shown in

Fig. 3A, there appeared a strong peak current (242.3 μA) when the formative branched polymer was treated without T_1 and T_2. While branched DNA polymer was treated with only T_1, a high LSV response (113.2 μA) was obtained, indicating that T_1 depolymerized the backbone of polymer (Fig. 3B). As demonstrated in Fig. 3C, T_2 merely dissociated the side chain of branched DNA polymer, resulting in a relatively higher signal (155.8 μA). However, when dual triggers T_1 and T_2 were simultaneously introduced to disassemble the backbone and side chain of polymer for realizing the efficient decomposition, a remarkably decreased electrochemical signal intensity (93.1 μA) was observed (Fig. 3D). The reason might be ascribed to the fact that our proposed strategy could improve decomposition efficiency, resulting in excellent analytical performance.

(Fig. 3)

3.4. Analytical performance of the biosensor for detection of Pb^{2+}

Under the optimized conditions, different concentrations of target Pb^{2+} were analyzed by the constructed electrochemical biosensor with LSV measurement. As shown in Fig. 4A, the LSV current response decreased with the increment of Pb^{2+} concentrations. A linear dependence between the peak currents and the logarithm of Pb^{2+} concentrations was acquired in the range from 1 pM to 100 nM with a detection limit of 0.24 pM (S/N = 3). The linear relationship could be represented as I = -29.159 lg$c$ + 124.151, with the correlation coefficient of r = 0.9980, where I and c represented the peak current intensity and Pb^{2+} concentration, respectively. In addition,

compared with other published Pb^{2+} detection methods (Table 2), the elaborated electrochemical biosensor provided a more effective approach with lower detection limit and wider dynamic concentration response range.

(Fig. 4)

(Table 2)

3.5. Selectivity and reproducibility of the biosensor

The selectivity of the constructed electrochemical biosensor was investigated by using Co^{2+}, Mg^{2+}, Cu^{2+} and Ni^{2+} (1 μM, respectively) as interfering metal ions under the same conditions. As shown in Fig. 5, the LSV responses were nearly in accordance with that of the blank sample when interfering metal ions were incubated alone. However, when 10 nM Pb^{2+} was coexisted with the interfering substances Co^{2+}, Mg^{2+}, Cu^{2+} and Ni^{2+}, only negligible changes were discovered compared to that of only Pb^{2+} existed. The satisfactory results revealed the high selectivity of this Pb^{2+} detection system. To further examine the reproducibility of the established assay, four repetitive experiments were carried out to measure 10 nM Pb^{2+} in 1.0 M KCl on the same electrode, and a relative standard deviation (RSD) of 4.3% was obtained, implying that the protocol was equipped with good reproducibility.

(Fig. 5)

3.6. Detection of Pb^{2+} in real samples

To further confirm the practicability of this electrochemical biosensor in real application, the recovery experimental trials were testified by standard addition methods. The water samples used in the study were tap water that collected from the Jialing River (Chongqing, China). Afterwards, the water samples spiked with Pb^{2+} at various concentrations of 1.00×10^{2}, 1.00, 1.00×10^{-1} and 1.00×10^{-3} nM were carried out using the established biosensor, and the corresponding results were demonstrated in Table 3. The recoveries varied from 95.40% to 103.00%, indicating potential applicability for the detection of Pb^{2+} with acceptable accuracy and reliability.

(Table 3)

4. Conclusion

In summary, by integrating the DNAzyme-aided target cyclic and in-situ generating AgNPs as electrochemical signal tag on programmable DNA structure, a sensitive branched DNA polymer sensing platform was proposed for Pb^{2+} detection. The merits of the biosensor contributed to several aspects: Firstly, under the cyclic process of Pb^{2+} cleavage, low number of target Pb^{2+} could generate abundant trigger T_1 and T_2, which could further participate in the disassembly of constructed polymer with higher sensitivity. Furthermore, in comparison to only one-trigger induced decomposition assay with inferior disassembly efficiency, the detection performance of our proposed assay was further improved with an efficient decomposition design, which was mainly contributed to the elimination of obstruction caused by dendritic

structure on electrode. In view of these advantages, the demonstrated method thus offered new opportunities for ultra-sensitively detecting other targets.

Acknowledgements

This work was financially supported by the National Natural Science Foundation (NNSF) of China (21505107, 21775124, 21575116, 51473136), and the Natural Science Foundation Project of Chongqing City (cstc2016jcyjA0189).

References

[1] F. Wang, C. H. Lu, I. Willner,
From cascaded catalytic nucleic acids to enzyme-DNA nanostructures: controlling reactivity, sensing, logic operations, and assembly of complex structures
Chem. Rev., 114 (2014), pp. 2881-2941.

[2] L. L. Yang, Y. Z. Tao, G. Y. Yue, R. B. Li, B. Qiu, L. H. Guo, Z. Y. Lin, H. H. Yang,
Highly selective and sensitive electrochemiluminescence biosensor for p53 DNA sequence based on nicking endonuclease assisted target recycling and hyperbranched rolling circle amplification
Anal. Chem., 88 (2016), pp. 5097-5103.

[3] S. Bi, M. Chen, X. Q. Jia, Y. Dong, Z. H. Wang,
Hyperbranched hybridization chain reaction for triggered signal amplification and concatenated logic circuits
Angew. Chem. Int. Ed., 54 (2015), pp. 8144-8148.

[4] L. Liu, J. W. Liu, H. Wu, X. N. Wang, R. Q. Yu, J. H. Jiang,
Branched Hybridization Chain Reaction Circuit for Ultrasensitive Localizable

Imaging of mRNA in Living Cells

Anal. Chem., 90 (2018), pp.1502-1505.

[5] X. F. Sun, H. H. Chen, S. L. Wang, Y. P. Zhang, Y. P. Tian, N. D. Zhou,

Electrochemical detection of sequence-specific DNA based on formation of G-quadruplex-hemin through continuous hybridization chain reaction

Analytica Chimica Acta, 1021 (2018), pp. 121-128.

[6] L. Li, C. C. Niu, T. Li, Y. F. Wan, Y. Zhou, H. J. Wang, R. Yuan, P. Liao,

Ultrasensitive electrochemiluminescence biosensor for detection of laminin based on DNA dendrimer-carried luminophore and DNA nanomachine-mediated target recycling amplification

Biosens. Bioelectron., 101 (2018), pp. 206-212.

[7] F. Xuan, I. M. Hsing,

Triggering hairpin-free chain-branching growth of fluorescent DNA dendrimers for nonlinear hybridization chain reaction

J. Am. Chem. Soc. 136 (2014), pp. 9810-9813.

[8] S. Bi, S. Z. Yue, S. S. Zhang,

Hybridization chain reaction: a versatile molecular tool for biosensing, bioimaging, and biomedicine

Chem. Soc. Rev., 46 (2017), pp. 4281-4298.

[9] L. P. Jia, S. S. Shi, R. N. Ma, W. L. Jia, H. S. Wang,

Highly sensitive electrochemical biosensor based on nonlinear hybridization chain reaction for DNA detection

Biosens. Bioelectron., 80 (2016), pp. 392-397.

[10] X. J. Ding, Y. H. Wang, W. Cheng, F. Mo, Y. Sang, L. L. Xu, S. J. Ding,

Aptamer based electrochemical adenosine triphosphate assay based on a

target-induced dendritic DNA nanoassembly

Microchim. Acta, 184 (2017), pp. 431-438.

[11] F. Xuan, T. W. Fan, I. M. Hsing,

Electrochemical interrogation of kinetically-controlled dendritic DNA/PNA assembly for immobilization-free and enzyme-free nucleic acids sensing

ACS nano, 9 (2015), pp. 5027-5033.

[12] Y. H. Wang, L. Jiang, Q. G. Leng, Y. H. Wu, X. X. He, K. M. Wang,

Electrochemical sensor for glutathione detection based on mercury ion triggered hybridization chain reaction signal amplification

Biosens. Bioelectron., 77 (2016), pp. 914-920.

[13] S. S. Lu, T. Hu, S. Wang, J. Sun, X. R. Yang,

Ultra-sensitive colorimetric assay system based on the hybridization chain reaction-triggered enzyme cascade amplification

ACS Appl. Mater. Interfaces, 9 (2017), pp. 167-175.

[14] W. B. Liang, Y. Zhuo, Y. N. Zheng, C. Y. Xiong, Y. Q. Chai, R. Yuan,

Electrochemiluminescent Pb^{2+}-driven circular etching sensor coupled to a DNA micronet-carrier

ACS Appl. Mater. Interfaces, 9 (2017), pp. 39812-39820.

[15] I. T. Hoffecker, N. Takemoto, Y. Arima, H. Iwata,

Sequence-specific nuclease-mediated release of cells tethered by oligonucleotide phospholipids

Biomaterials, 53 (2015), pp. 318-329.

[16] J. P. Magnusson, F. Fernández-Trillo, G. Sicilia, S. G. Spain, C. Alexander,

Programmed assembly of polymer-DNA conjugate nanoparticles with optical readout and sequence-specific activation of biorecognition

Nanoscale, 6 (2014), pp. 2368-2374.

[17] R. Z. Peng, H. J. Wang, Y. F. Lyu, L. J. Xu, H. Liu, H. L. Kuai, W. H. Tan,

Facile assembly/disassembly of DNA nanostructures anchored on cell-mimicking giant vesicles

J. Am. Chem. Soc., 139 (2017), pp. 12410-12413.

[18] Z. Li, X. W. He, X. C. Luo, L. Wang, N. Ma,

DNA-programmed quantum dot polymerization for ultrasensitive molecular imaging of cancer cells

Anal. Chem., 88 (2016), pp. 9355-9358.

[19] C. W. Brown III, S. Buckhout-White, S. A. Díaz, J. S. Melinger, M. G. Ancona, E. R. Goldman, I. L. Medintz,

Evaluating dye-labeled DNA dendrimers for potential applications in molecular biosensing

ACS Sens., 2 (2017), pp. 401-410.

[20] Y. Chen, M. L. Yang, Y. Xiang, R. Yuan, Y. Q. Chai,

Binding-induced autonomous disassembly of aptamer-DNAzyme supersandwich nanostructures for sensitive electrochemiluminescence turn-on detection of ochratoxin A

Nanoscale, 6 (2014), pp. 1099-1104.

[21] H. M. Da, H. Y. Liu, Y. N. Zheng, R. Yuan, Y. Q. Chai,

A highly sensitive $VEGF_{165}$ photoelectrochemical biosensor fabricated by assembly of aptamer bridged DNA networks

Biosens. Bioelectron., 101 (2018), pp. 213-218.

[22] N. C. Chen, X. C. Shi, Y. Wang,

Molecularly regulated reversible DNA polymerization

Angew. Chem. Int. Ed. 55 (2016), pp. 6657-6661.

[23] L. L. Liang, F. F. Lan, S. G. Ge, J. H. Yu, N. Ren, M. Yan,

Metal-enhanced ratiometric fluorescence/naked eye bimodal biosensor for lead ions analysis with bifunctional nanocomposite probes

Anal. Chem., 89 (2017), pp. 3597-3605.

[24] Y. J. Yu, C. Yu, Y. Z. Niu, J. Chen, Y. L. Zhao, Y. C. Zhang, R. F. Gao, J. L. He,

Target triggered cleavage effect of DNAzyme: Relying on Pd-Pt alloys functionalized Fe-MOFs for amplified detection of Pb^{2+}

Biosens. Bioelectron., 101 (2018), pp. 297-303.

[25] G. Frens,

Controlled nucleation for the regulation of the particle size in monodisperse gold suspensions

Nature, 241 (1973), pp. 20-22.

[26] M. Rizwan, S. Elma, S. A. Lim, M. U. Ahmed,

AuNPs/CNOs/SWCNTs/chitosan-nanocomposite modified electrochemical sensor for the label-free detection of carcinoembryonic antigen

Biosens. Bioelectron., 107 (2018), pp. 211-217.

[27] C. Y. Wang, X. X. Ye, Z. G. Wang, T. Wu, Y. Y. Wang, C. Y. Li,

Molecularly imprinted photo-electrochemical sensor for human epididymis protein 4 based on polymerized ionic liquid hydrogel and gold nanoparticle/ZnCdHgSe quantum dots composite film

Anal. Chem., 89 (2017), pp. 12391-12398.

[28] X. N. Fang, Y. Liu, L. Jimenez, Y. K. Duan, G. B. Adkins, L. Qiao, B. H. Liu, W. W. Zhong,

Rapid enrichment and sensitive detection of multiple metal ions enabled by

macroporous graphene foam

Anal. Chem., 89 (2017), pp. 11758-11764.

[29] Y. Shi, H.Y. Wang, X. X. Jiang, B. Sun, B. Song, Y. Y. Su, Y. He,

Ultrasensitive, specific, recyclable, and reproducible detection of lead ions in real systems through a polyadenine-assisted, surface-enhanced raman scattering silicon chip

Anal. Chem., 88 (2016), pp. 3723-3729.

[30] W. Yun, D. Z. Cai, J. L. Jiang, P. X. Zhao, Y. Huang, G. Sang,

Enzyme-free and label-free ultra-sensitive colorimetric detection of Pb^{2+} using molecular beacon and DNAzyme based amplification strategy

Biosens. Bioelectron., 80 (2016), pp. 187-193.

[31] L. Cui, J. Wu, J. Li, H. X. Ju,

Electrochemical sensor for lead cation sensitized with a DNA functionalized Porphyrinic metal-organic framework

Anal. Chem., 87 (2015), pp. 10635-10641.

[32] X. Wang, C. L. Yang, S. J. Zhu, M. Yan, S. G. Ge, J. H. Yu,

3D origami electrochemical device for sensitive Pb^{2+} testing based on DNA functionalized iron-porphyrinic metal-organic framework

Biosens. Bioelectron., 87 (2017), pp. 108-11

[33] L. L. Wang, Y. L. Wen, L. Y. Li, X. Yang, N. Q. Jia, W. Li, J. R. Meng, M. L. Duan, X. G. Sun, G. Liu,

Sensitive and label-free electrochemical lead ion biosensor based on a DNAzyme triggered G-quadruplex/hemin conformation

Biosens. Bioelectron., 115 (2018) pp. 91-96.

[34] F. M. Liu, Y. Zhang, W. Yin, C. J. Hou, D. Q. Huo, B. He, L. L. Qian, H. B. Fa, **A high-selectivity electrochemical sensor for ultra-trace lead (II) detection based on a nanocomposite consisting of nitrogen-doped graphene/gold nanoparticles functionalized with ETBD and Fe_3O_4@TiO_2 core-shell nanoparticles** Sensors and Actuators B, 242 (2017) pp. 889-896.

[35] Y. J. Yu, C. Yu, Y. Z. Niu, J. Chen, Y. L. Zhao, Y. C. Zhang, R. F. Gao, J. L. He, **Target triggered cleavage effect of DNAzyme: Relying on Pd-Pt alloys functionalized Fe-MOFs for amplified detection of Pb^{2+}** Biosens. Bioelectron., 101 (2018), pp. 297-303.

Figures caption

Scheme 1. (A) Preparation of DNA triggers (T_1 and T_2), (B) schematic illustration of the triggers induced disassembly of branched DNA polymer for the ultrasensitive determination of Pb^{2+}.

Fig. 1. CV and EIS response of different modified electrodes: (a) bare GCE; (b) depAu/GCE; (c) DI/depAu/GCE; (d) HT/DI/depAu/GCE; (e) DMs/HT/DI/depAu/GCE; (f) incubation of T_1 + T_2 /DMs/HT/DI/depAu/GCE in 5.0 mM $[Fe(CN)_6]^{3-/4-}$.

Fig. 2. (A) Optimum time of Pb^{2+} cleavage in Pb^{2+}-dependent DNAzyme. (B) Optimum incubation time of triggers (T_1 and T_2) for inducing branched DNA polymer disassembly. All the electrochemical signal response was detected in 1.0 M KCl.

Fig. 3. LSV responses toward different dissociation means: (A) without decomposition, (B) T_1 decomposition, (C) T_2 decomposition and (D) T_1 and T_2 decomposition.

Fig. 4. (A) The LSV responses of the biosensor for the determination of Pb^{2+} with a series of concentrations: (a) 1 pM, (b) 2 pM, (c) 10 pM, (d) 40 pM, (e) 100 pM, (f) 1 nM, (g) 10 nM, and (h) 100 nM. (B) LSV calibration curve of the biosensor for Pb^{2+} detection. The error bars represent the standard deviation of three separate assays (n = 3).

Fig. 5. Selectivity of the developed biosensor for 10 nM Pb^{2+} and 1 μM other metal ions including Co^{2+}, Mg^{2+}, Cu^{2+}, Ni^{2+}, and a mixture of Pb^{2+} and the interference metal ions.

415

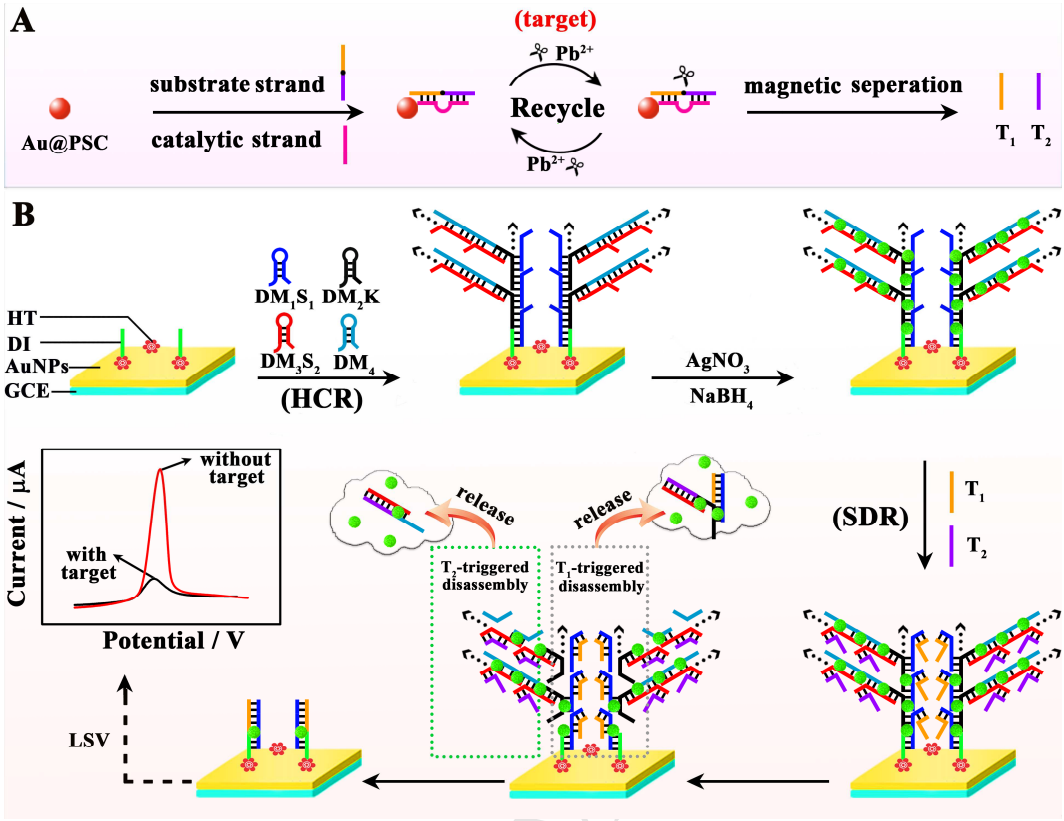

416

417 **Scheme 1**

418

419

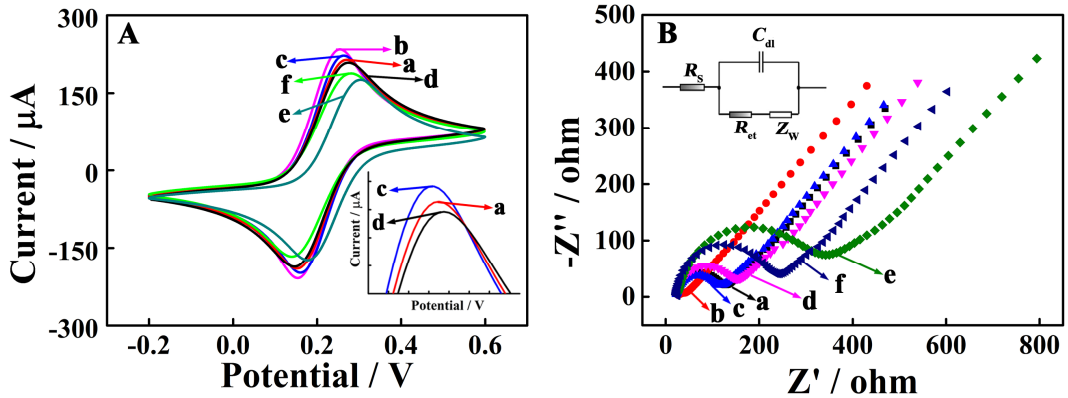

420

421 **Fig. 1**

422

423

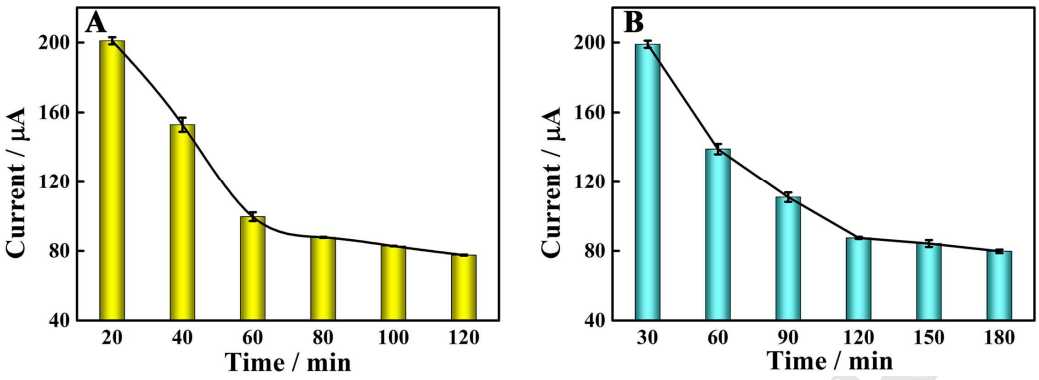

424

425 **Fig. 2**

426

427

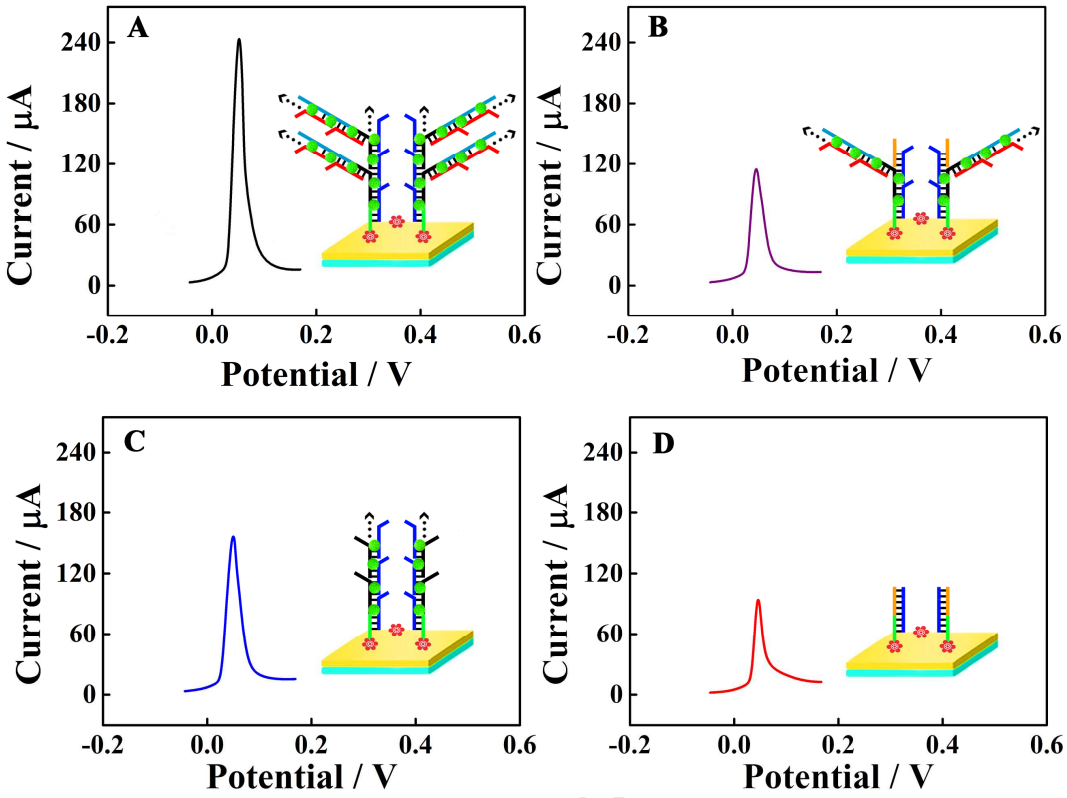

428

429 **Fig. 3**

430

431

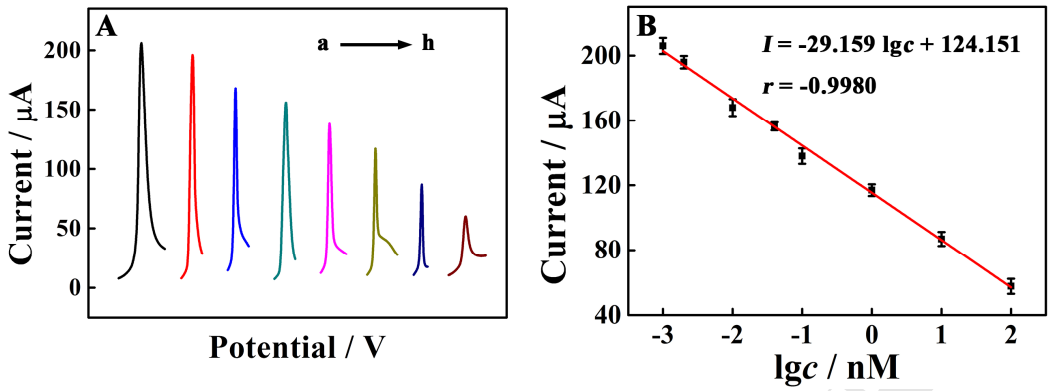

432

433 **Fig. 4**

434

435

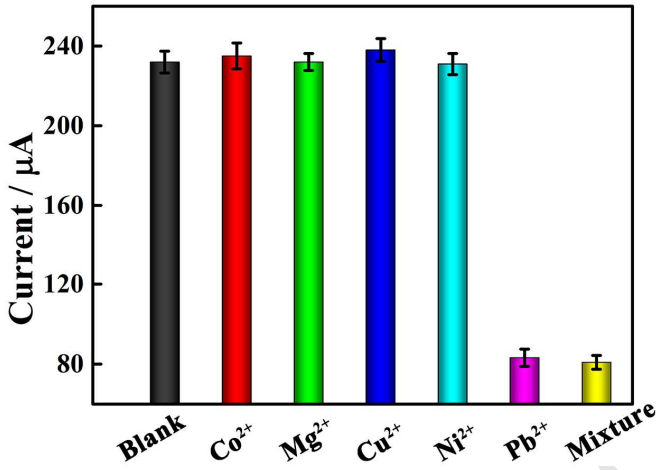

436

437 **Fig. 5**

438

Table caption

Table 1. List of all DNA sequences employed in this study.

Table 2. The performance comparison of present work with reported methods for Pb^{2+} detection.

Table 3. Results of determination Pb^{2+} in water sample and recovery test.

445 **Table 1.** List of all DNA sequences employed in this study.

Name	Sequence (5'→3')
DI	CCT CAT CCC ACT CCT ACC TAA ACC AAA AA-SH
DM_1S_1	GGT TTA GGT AGG AGT GGG ATG AGG CCA AAT CCT CAT CCC ACT CCT ACC CAT CTC TTC C
DM_2K	CCA CTC ACT CAC CTC ACC TTC AAC CTT CAC CTC ATC CCA CTC CTA CCT AAA CCG GTA GGA GTG GGA TGA GGA TTT GG
DM_3S_2	GTT GAA GGT GAG GTG AGT GAG TGG CCA CTT CCA CTC ACT CAC CTC ACC CTA AAT CCA C
DM_4	CCA CTC ACT CAC CTC ACC TTC AAC GGT GAG GTG AGT GAG ACT CAC TAT
Catalytic Strand	HS-$(CH_2)_6$-CAT CTC TTC TCC GAG CCG GTC GAA ATA GTG AGT
Substrate Strand	GTG GAT TTA GGG TGA GGT GAG TGA GAC TCA CTA TrA GGA AGA GAT GGG TAG GAG TGG GAT GAG GAT TTG G

446

447 **Table 2.** The performance comparison of present work with reported methods for Pb^{2+}
448 detection.

Method for analysis	Detection limit	Linear range	Reference
Fluorescence	50 pM	50 pM - 500 pM	[28]
Surface-enhanced Raman scattering	8.9 pM	10 pM - 1 μM	[29]
Colorimetry	20 pM	50 pM - 5 nM	[30]
Electrochemistry	34 pM	50 pM - 200 nM	[31]
Electrochemistry	20 pM	30 pM - 1000 nM	[32]
Electrochemistry	8 pM	10 pM - 1000 nM	[33]
Electrochemistry	0.75 pM	4 pM - 20 nM	[34]
Electrochemistry	2 pM	5 pM - 1000 nM	[35]
Electrochemistry	0.24 pM	1 pM - 100 nM	This work

449

450 **Table 3.** Results of determination Pb^{2+} in water sample and recovery test.

Sample	Added/(nM)	Found/(nM)	Recovery/%	RSD/%
1	1.00×10^{2}	1.027×10^{2}	102.70	3.4
2	1.00	9.85×10^{-1}	98.50	4.5
3	1.00×10^{-1}	9.54×10^{-2}	95.40	2.1
4	1.00×10^{-3}	1.03×10^{-3}	103.00	3.7

451

Table caption

Table 1. List of all DNA sequences employed in this study.

Table 2. The performance comparison of present work with reported methods for Pb^{2+} detection.

Table 3. Results of determination Pb^{2+} in water sample and recovery test.

Table 1. List of all DNA sequences employed in this study.

Name	Sequence (5'→3')
DI	CCT CAT CCC ACT CCT ACC TAA ACC AAA AA-SH
DM_1S_1	GGT TTA GGT AGG AGT GGG ATG AGG CCA AAT CCT CAT CCC ACT CCT ACC CAT CTC TTC C
DM_2K	CCA CTC ACT CAC CTC ACC TTC AAC CTT CAC CTC ATC CCA CTC CTA CCT AAA CCG GTA GGA GTG GGA TGA GGA TTT GG
DM_3S_2	GTT GAA GGT GAG GTG AGT GAG TGG CCA CTT CCA CTC ACT CAC CTC ACC CTA AAT CCA C
DM_4	CCA CTC ACT CAC CTC ACC TTC AAC GGT GAG GTG AGT GAG ACT CAC TAT
Catalytic Strand	HS-$(CH_2)_6$-CAT CTC TTC TCC GAG CCG GTC GAA ATA GTG AGT
Substrate Strand	GTG GAT TTA GGG TGA GGT GAG TGA GAC TCA CTA TrA GGA AGA GAT GGG TAG GAG TGG GAT GAG GAT TTG G

Table 2. The performance comparison of present work with reported methods for Pb^{2+} detection.

Method for analysis	Detection limit	Linear range	Reference
Fluorescence	50 pM	50 pM - 500 pM	[28]
Surface-enhanced Raman scattering	8.9 pM	10 pM - 1 μM	[29]
Colorimetry	20 pM	50 pM - 5 nM	[30]
Electrochemistry	34 pM	50 pM - 200 nM	[31]
Electrochemistry	20 pM	30 pM - 1000 nM	[32]
Electrochemistry	8 pM	10 pM - 1000 nM	[33]
Electrochemistry	0.75 pM	4 pM - 20 nM	[34]
Electrochemistry	2 pM	5 pM - 1000 nM	[35]
Electrochemistry	0.24 pM	1 pM - 100 nM	This work

Table 3. Results of determination Pb^{2+} in water sample and recovery test.

Sample	Added/(nM)	Found/(nM)	Recovery/%	RSD/%
1	1.00×10^{2}	1.027×10^{2}	102.70	3.4
2	1.00	9.85×10^{-1}	98.50	4.5
3	1.00×10^{-1}	9.54×10^{-2}	95.40	2.1
4	1.00×10^{-3}	1.03×10^{-3}	103.00	3.7

Figures caption

Scheme 1. (A) Preparation of DNA triggers (T_1 and T_2), (B) schematic illustration of the triggers induced disassembly of branched DNA polymer for the ultrasensitive determination of Pb^{2+}.

Fig. 1. CV and EIS response of different modified electrodes: (a) bare GCE; (b) depAu/GCE; (c) DI/depAu/GCE; (d) HT/DI/depAu/GCE; (e) DMs/HT/DI/depAu/GCE; (f) incubation of T_1 + T_2 /DMs/HT/DI/depAu/GCE in 5.0 mM $[Fe(CN)_6]^{3-/4-}$.

Fig. 2. (A) Optimum time of Pb^{2+} cleavage in Pb^{2+}-dependent DNAzyme. (B) Optimum incubation time of triggers (T_1 and T_2) for inducing branched DNA polymer disassembly. All the electrochemical signal response was detected in 1.0 M KCl.

Fig. 3. LSV responses toward different dissociation means: (A) without decomposition, (B) T_1 decomposition, (C) T_2 decomposition and (D) T_1 and T_2 decomposition.

Fig. 4. (A) The LSV responses of the biosensor for the determination of Pb^{2+} with a series of concentrations: (a) 1 pM, (b) 2 pM, (c) 10 pM, (d) 40 pM, (e) 100 pM, (f) 1 nM, (g) 10 nM, and (h) 100 nM. (B) LSV calibration curve of the biosensor for Pb^{2+} detection. The error bars represent the standard deviation of three separate assays (n = 3).

Fig. 5. Selectivity of the developed biosensor for 10 nM Pb^{2+} and 1 μM other metal ions including Co^{2+}, Mg^{2+}, Cu^{2+}, Ni^{2+}, and a mixture of Pb^{2+} and the interference metal ions.

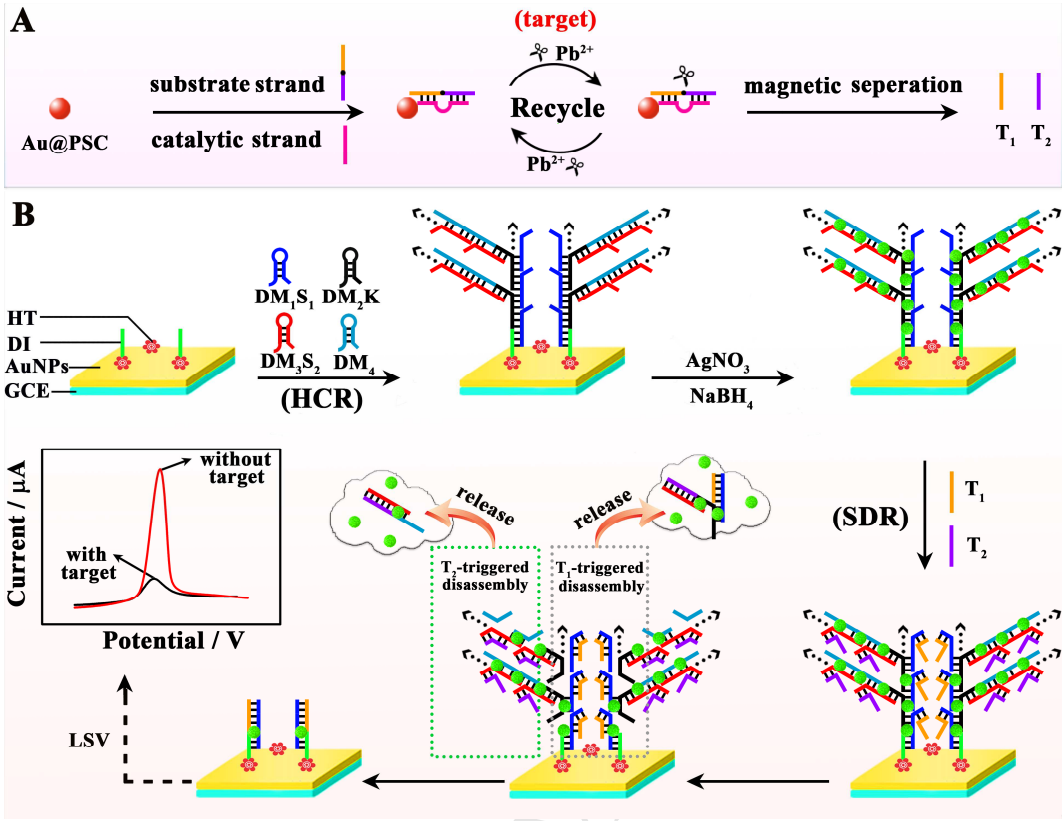

Scheme 1

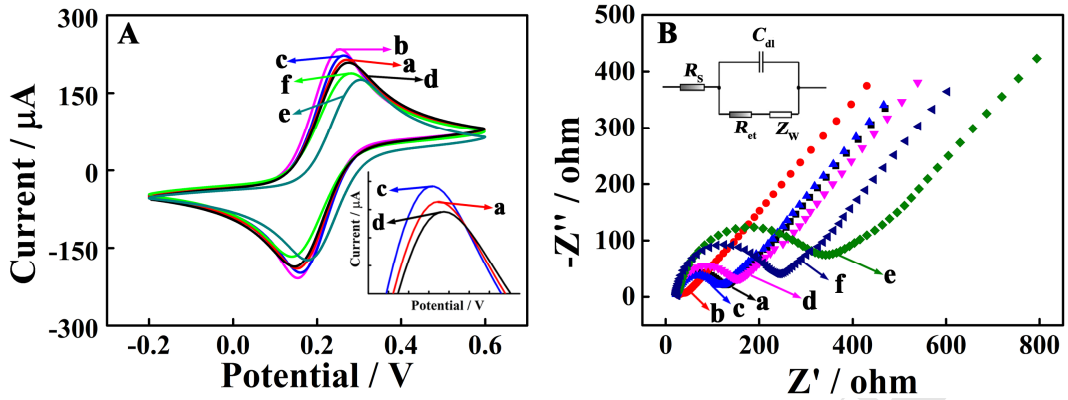

Fig. 1

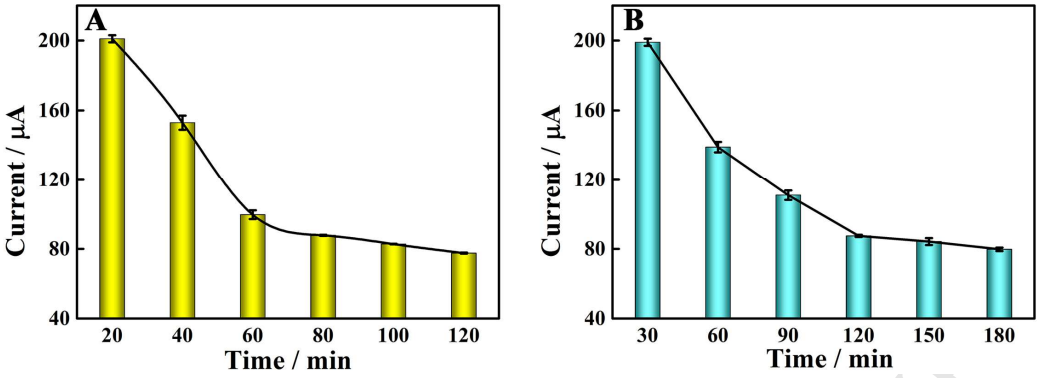

Fig. 2

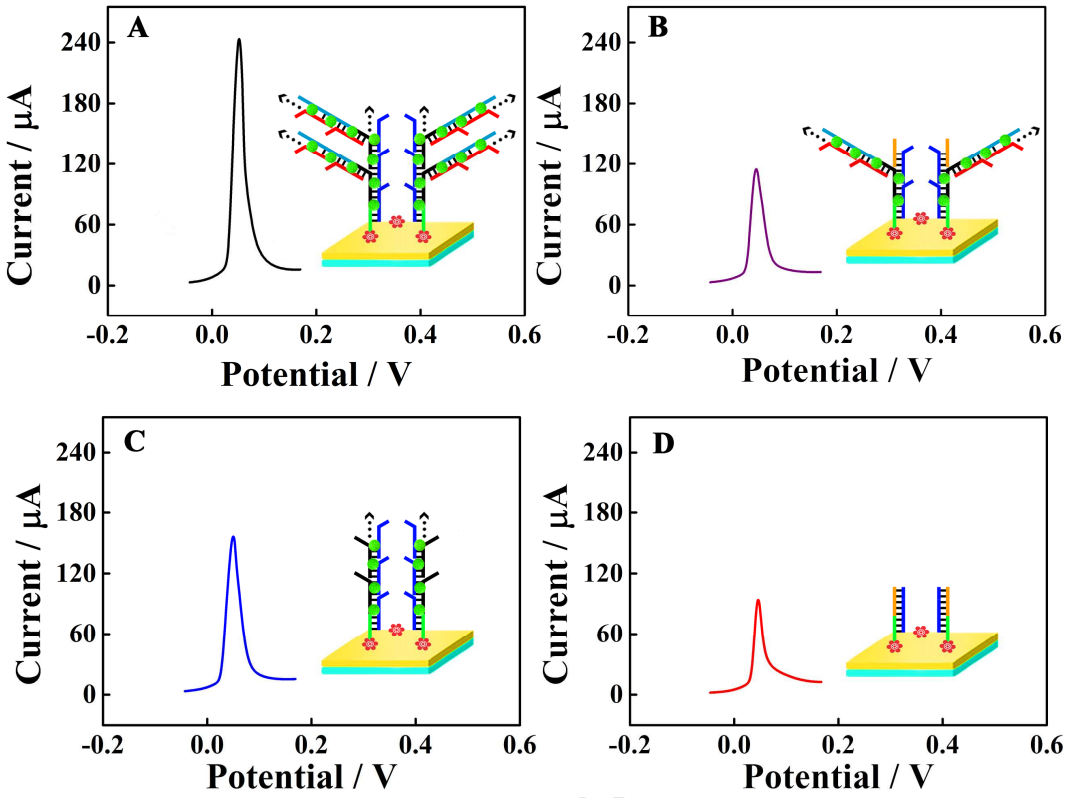

Fig. 3

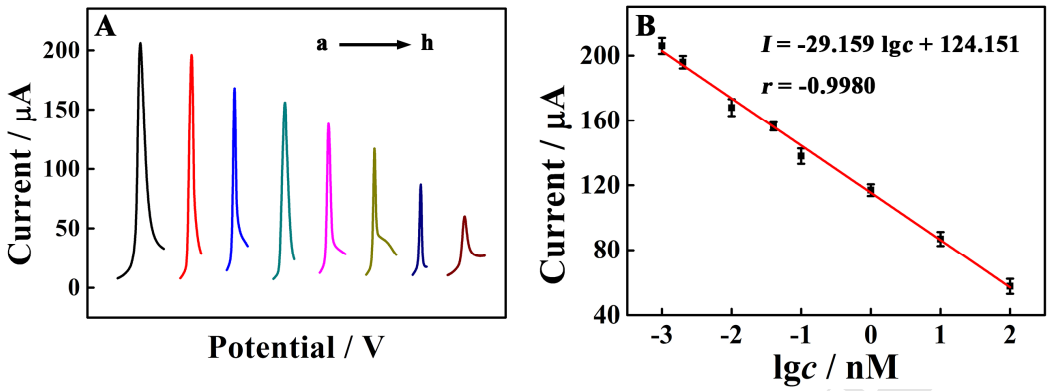

Fig. 4

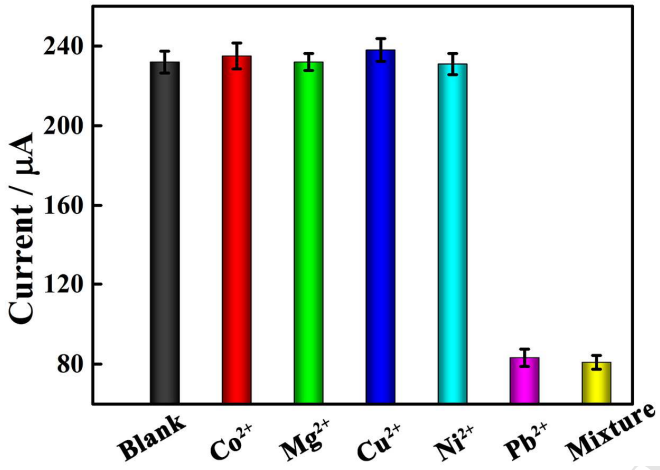

Fig. 5

Highlights

- A novel label-free and ultrasensitive biosensor based on the dual triggers induced DNA polymer disassembly was developed for Pb^{2+} detection.
- The proposed approach exhibited higher decomposition efficiency compared with conventional one-trigger induced disassembly strategy.
- The Pb^{2+}-dependent DNAzyme was introduced for target-transition recycling amplification to promote detection sensitivity.
- The fabricated electrochemical biosensor exhibited excellent sensitivity, good selectivity, and acceptable reproducibility.